Journal of Colloid and Interface Science 413 (2014) 159–166

Contents lists available at ScienceDirect

Journal of Colloid and Interface Science

www.elsevier.com/locate/jcis

Time and frequency dependent rheology of reactive silica gels

Miao Wang [a,b], H. Henning Winter [b], Günter K. Auernhammer [a,*]

[a] Max-Planck Institute for Polymer Research, Ackermannweg 10, Mainz, Germany
[b] Chemical Engineering, University of Massachusetts, Amherst, MA, USA

ARTICLE INFO

Article history:
Received 19 June 2013
Accepted 18 September 2013
Available online 2 October 2013

Keywords:
Silica gel
Rheology
Structural relaxation

ABSTRACT

In a mixture of sodium silicate and low concentrated sulfuric acid, nano-sized silica particles grow and may aggregate to a system spanning gel network. We studied the influence of the finite solubility of silica at high pH on the mechanical properties of the gel with classical and piezo-rheometers. Direct preparation of the gel sample in the rheometer cell avoided any pre-shear of the gel structure during the filling of the rheometer. The storage modulus of the gel grew logarithmically with time with two distinct growth laws. The system passes the gel point very quickly but still shows relaxation at low frequency, typically below 6 rad/s. We attribute this as a sign of structural rearrangements due to the finite solubility of silica at high pH. The reaction equilibrium between bond formation and dissolution maintains a relatively large bond dissolution rate, which leads to a finite life time of the bonds and behavior similar to physical gels. This interpretation is also compatible with the logarithmic time dependence of the storage modulus. The frequency dependence was more pronounced for lower water concentrations, higher temperatures and shorter reaction times. With two relaxation models (the modified Cole–Cole model and the empirical Baumgaertel–Schausberger–Winter model) we deduced characteristic times from the experimental data. Both models approximately described the data and resulted in similar relaxation times.

1. Introduction

Aggregated colloids (colloidal gels) are important in everyday life and for fundamental research. The tunability of the system and the analogy to atomic systems have motivated a strong scientific interest in the dynamic behavior of colloidal gels [1–5]. In colloidal and molecular systems gelation is introduced by attractive interactions between the constituents (molecules, colloids or even more complex hierarchical structures like crystallites). The detailed mechanism may differ significantly from system to system. According to the durability of the bond between the constituents, gels are often classified as either chemical [6,7] or physical gels [8–11], where chemical gels are assumed to have bonds of an infinite life time and physical gels have bonds of a finite life time. For both, the constituents aggregate and the growth of clusters eventually leads to the formation of a system spanning network. Often the state of a gel depends on its history, i.e., the system is non-ergodic. Whereas chemical gels typically approach a final state, physical gels get trapped in non-equilibrium states and tend to age even after long periods of time.

Similarities between physical and chemical gels have been demonstrated by many studies. In the percolation model, the gel point is defined as the time, when the ratio between the real and imaginary part of the shear modulus, i.e., the loss tangent, is independent of the frequency. This behavior has been found in polymer (chemical) gels [12,13] and physical gels [14,15]. The physical gel of PVC plastisols exhibits the same power law relaxation as a chemically cross-linking system [15]. Furthermore, physical gels and glassy systems were often compared in the literature. It was reported that the dynamics of gelatin gels (physical gel) share characteristics with glassy systems on ergodic-to-non-ergodic transition kinetics [16], memory [17] and aging [18] effects. The relaxation to a non-ergodic background in gelatin gel was also found to be very similar to the relaxation pattern in glasses [19].

Besides the scientific interest, further understanding of gel systems has considerable impact for industry. Inorganic particles are widely used as filler particles in many applications. Examples include plastic parts, paints, coatings, pharmaceuticals, cosmetics, and food products. A cheap and efficient way of making such filler particles is to synthesize particle aggregates and mill them afterwards to the desired size. A prominent example is precipitated silica gel, also called silicic acid gel. Almost spherical silica particles are formed by fragmentation of the gel [20,21].

The characterization of precipitated silica gel began already in the 1920s [22]. In a series of the studies, Hurd discussed the influence of reactant variations [23,24] and temperature [25] on the gelation time. The chemical process and gelation phenomenon were detailed by Iler and Brinker [20,26]. By acidifying a soluble silicate, the silicic acid is firstly formed, which then reacts to form

* Corresponding author. Fax: +49 6131 379 100.
E-mail address: auhammer@mpip-mainz.mpg.de (G.K. Auernhammer).

0021-9797/$ - see front matter © 2013 Elsevier Inc. All rights reserved.
http://dx.doi.org/10.1016/j.jcis.2013.09.035

primary particles by condensation. The suspended particles grow further and aggregate with each other. That leads to a particle network, which extends throughout the system and forms a gel [20,27].

The time-dependence of the viscosity was investigated for the precipitated silica gel before its gel point by rheological measurement. Two stages were noted: a slow increase of viscosity during the preliminary stage, which was attributed to the formation of colloidal particles, followed by a rapid viscosity growth, for which the particle size determines the rate [28].

The relaxation processes in silica gels were studied theoretically [29] and experimentally by the 3-point bending method [30,31]. Wet gel bar samples were immersed in the bath of their medium liquid and the modulus was measured as the load required to produce a constant deflection [32]. The relaxation is understood as the sum of hydrodynamic and viscoelastic relaxation, which is caused by flow of the liquid medium in the system and irreversible deformation of the network under load. The chemical attack, i.e., hydrolysis, of the medium liquid on the gel was believed to be the reason for the relaxation in silica gel. When there is water in the medium, the silica bonds dissociate in the water (bond breakage) [30].

Our study focuses on the time and frequency dependent dynamic moduli of precipitated silica gel. The rheological properties of our silica gel exhibited a number of similarities to physical gels and weak colloidal gels. We observed a logarithmic growth of the storage modulus with time as previously found with physical gels [15,18]. This logarithmic time dependence is usually attributed to bond reversibility which can lead to a structural change, different from a chemical gel. The dynamic similarity between precipitated silica gels and physical gels was also found in the frequency sweep test. In comparison, a gel of chemically bound hard particles is expected to show a constant, frequency independent storage modulus at low frequencies, since the relaxation time exceeds the experimental time window [33,34]. The experiments we performed were at concentrations close to the percolation threshold, i.e., close to the minimal concentration of reactants, which is necessary to form a system spanning network. The behavior of the system was sensitive to external parameters. The influence of water concentration, temperature and time on the frequency dependence was studied. To understand the frequency dependence further, we applied two relaxation models: the modified Cole–Cole and Baumgaertel–Schausberger–Winter (BSW) models to analyse the experimental data.

In the discussion, we concentrate on the following points: 1. Is the precipitated silica gel at high pH-value a "real" chemical gel? 2. Can the relaxation models developed for polymer systems describe the relaxation behavior of silica gel? 3. Are there any unifying relaxation features for the silica gel in comparison to physical gel behavior?

2. Material and methods

2.1. Material

The reactants are sodium silicate solution (Natronwasserglas 37/40°, 40 wt.%, kindly provided by KRUSE-GROUP, Hanau, Germany) and sulfuric acid (96.4 wt.%, Fisher Scientific GmbH, Schwerte, Germany), which was diluted with milli-Q water to 3.2 wt.%. All reactants were used as provided without further purification. The sodium silicate has a molar SiO_2:Na_2O ratio of 3.3, which is typical for the production of precipitated silica and gels. The volume ratio between the sodium silicate solution and the diluted sulfuric acid solution was fixed as 1:2. As detailed below, if desired, the solution was further diluted with milli-Q water. The concentrations were chosen to adjust the gelation time in an experimentally accessible time window. Depending on the water content, the time to form a gel varied from about 20 min to 5 h, long enough to prevent gelation during experiment preparation, and short enough to efficiently avoid evaporation (see below). All samples originated from the same batch of sodium silicate to avoid batch-to-batch variations.

Silica gel without additional water was alkaline with a pH-value of 11.0 ± 0.1 at room temperature T = 23 °C, as measured with a pH-meter (Lab 850, Schott Instruments, Mainz, Germany). The pH-value remained constant during the reaction. The pH-value decreased to 10.9 ± 0.1 when the temperature was increased to 50 °C.

The solubility of silica in water increases strongly with pH [28]. Silica bonds can dissolve at pH-values above 9. The silica gel becomes reactive and quickly assumes a reaction equilibrium. The chemical reactions involved have been described in detail previously [20,21,35] and can be written as [35]:

$$Na_2O \cdot xSiO_2 + H_2SO_4 \rightleftharpoons xSiO_2 + Na_2SO_4 + H_2O$$

with x = 3.3 in this study. The appearance of the sample changed from a transparent and colorless solution immediately after preparation to a slightly turbid solid at the gel point to a white gel after several hours. The gel consisted of aggregates of primary particles, which were visible in scanning electron microscopy (SEM) images (Fig. 1A). The image illustrates the typical size of aggregates with diameters of 60–130 nm. The sample for SEM was prepared 1 h after mixing the reactants and was then kept at T = 100 °C for 3 days in a vacuum oven to remove the water from the sample.

In order to investigate the influence of the reactant concentration, extra water was added to the reaction mixture. We denoted the amount of extra water by the ratio R, defined as the additional water volume divided by the total solution volume (including the additional water).

$$R = \frac{V_{additional\ H_2O}}{V_{solution}} \quad (1)$$

We varied R from 0% to 20%. The silica volume fraction in the samples with R = 0%, 10% and 20% were 8.6%, 7.3% and 6.3%, respectively. The pH-value at T = 23 °C decreased from 11.0 ± 0.1 for R = 0 to 10.9 ± 0.1 for R = 20%. By slightly decreasing the pH value, additional water shifts the reaction equilibrium in the direction of undissolved silica bonding since silica solubility decreases. Furthermore, the temperature controls the rate at which bonds form and open. So the life time of the silica bonds can be adjusted by these parameters.

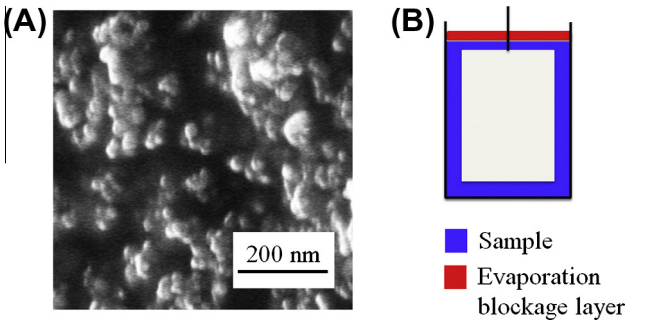

Fig. 1. (A): SEM image of the silica gel. The sample was prepared 1 h after mixing of the reactants and kept at T = 100 °C for 3 days in a vacuum oven for complete drying. (B): Setup of rheometer Couette cell with sample (blue) and evaporation blockage layer (red). The inner cylinder rotated oscillatorilly. (For interpretation of the references to color in this figure legend, the reader is referred to the web version of this article.)

2.2. Experimental method

The rheological experiments were performed in a strain controlled rheometer (ARES-LS, Rheometric Scientific Inc., Piscataway, NJ, USA) equipped with a Couette cell and also a homemade piezo-rheometer. For the ARES rheometer, the diameters of cup and inner bob are 27.0 mm and 25.0 mm, respectively, and the length of bob is 32.0 mm. The sample volume was 2.61 ml. The experiments were performed in the strain-controlled oscillatory mode to obtain the frequency dependent storage modulus G' and loss modulus G''. A strain of $\gamma = 0.0005$ was chosen (see below), to avoid strain-induced changes in the sample. Due to this low strain the resolution limit of the transducer (0.02 g cm) corresponded to a lowest measurable complex modulus of 115 Pa.

After mixing for 30 s, the reactants were filled into the rheometer cup. It was checked by visual inspection that no air bubbles were in the system. Immiscible oil was placed as an evaporation barrier on the exposed top surface of the sample (Fig. 1B). With this method, no evaporation effects were observed during the measurements. Since the oil was immiscible with the water-based solution, it stayed at the top of the sample and did not affect the measurement results.

Alternative rheological measurements were performed with a homemade piezo-rheometer, which functions as a strain-controlled plate-plate rheometer. A piezo actuator applies a defined shear strain on the sample. A second piezo actuator detects the stress propagated through the sample [36–38]. Details about our homemade piezo-rheometer were reported by Roth et al. [39]. We used a gap distance of 100 μm. A 15 μL sample was placed between the two parallel glass substrates. As an evaporation blockage layer, polydimethylsiloxane (molecular weight approx. 8000 g/mol) was filled around the sample. We checked that the evaporation barrier had no measurable contribution to the results reported in this work.

The preparation of the sample (mixing, inserting into the rheometer, adding the evaporation blockage layer, starting the data acquisition) lasted typically 2 min. Slight differences (less than 2 min) of experiment preparation time and composition of the samples could not be excluded for each individual measurement. Since acquisition times were at least several thousands of seconds, these time differences were negligible. To prevent any shear history effects all samples were filled into the rheometer in the sol state. For this reason no sample was used with gelation times shorter than 5 min.

3. Results

In the following we present results as a function of time, frequency, composition, temperature, and reaction time. First we determined the maximum allowed strain for a linear response to be $\gamma = 0.0035$. Below this value the mechanical response of the sample did not depend on the applied strain amplitude (Supplementary material, Fig. S1). A strain $\gamma = 0.0005$ was chosen for all measurements to ensure that all data was collected in the linear regime. The gelation process was then followed by either measuring at a fixed frequency of $\omega = 10$ rad/s (time sweep) or by repeatedly taking mechanical spectra in the frequency range of $\omega = 0.1$–30 rad/s (frequency sweeps). The time sweep data gave us the time dependence up to 10^4 s. From the frequency sweep data we could analyze the evolution of the frequency dependence.

3.1. Time dependence

The experiments show a number of common features in the gelation behavior, which we first describe on the example of the silica gel with $R = 0$ and at $T = 23$ °C. Moduli of the gel were measured with time sweep and repeated frequency sweeps. With the help of time-resolved rheometry [40], the temporal evolution of the storage modulus G' and the loss modulus G'' were obtained from the repeated frequency sweeps. From the repeated frequency sweeps, the data points measured at $\omega = 10$ rad/s were extracted and plotted as a function of time (Fig. 2 squares). Then they were compared with time sweep results (Fig. 2 circles). The good agreement of both curves demonstrated the compatibility of these two experimental methods. A linear relation between the mechanical moduli (G', G'') and the logarithm of the reaction time t was measured (Fig. 2C). This feature is also typical for physical gels [15,18], see also Section 4.1.

In Fig. 3, the storage modulus G' and loss modulus G'' are plotted as function of time t for different compositions. An increase of additional water from 0% to 20% shifted the modulus growth curve to longer times by about one decade. This demonstrates the high sensitivity of the gelation process to the gel composition. Such a strong influence of the concentration on the gelation time is expected, since the experiments were carried out at concentrations close to the percolation threshold.

At the chosen strain, the response of the sol and the early gel were below the resolution limit of the rheometer (Section 2.2) and could not be measured. Consequently, the gel point was not directly observable.

The overall shape of the time evolution was more or less independent of composition (Fig. 3A). To account for the change in time scale, we introduced a characteristic time of the gel formation (Fig. 3B). It turned out to be helpful to fit the storage modulus in the range below 600 Pa with a logarithmic time dependence.

$$G' = A \cdot \log\left(\frac{t}{t_{char}}\right), \tag{2}$$

where A and t_{char} are fit parameters. The x-axis intercept of the fitted line (the extrapolation of the fit is set to 0) is defined as the characteristic time t_{char}. This characteristic time is also connected with (but not identical to) the gelation time, as defined through rheological data taken while passing the gel point. We assume that t_{char} and the gelation time show the same dependencies (Fig. 3C).

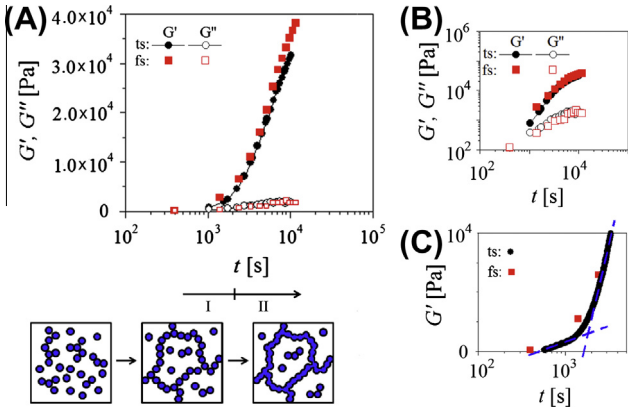

Fig. 2. The growth of the moduli for a gel with $R = 0$ at $\gamma = 0.0005$, $T = 23$ °C, and $\omega = 10$ rad/s in linear-log (A) and log–log representation (B). In the time sweep (ts, circles) only one out of 50 data points is shown. With a repeated frequency sweeps (fs, squares), moduli were measured in the frequency range from 0.1 to 30 rad/s. Only points for $\omega = 10$ rad/s are shown. (C): Zoom of the data at low storage modulus range ($G' < 10^4$ Pa). All data points of the time sweep are shown. The fit lines (dashed) show the linear relation between G' and log (t). The intersection of both fits gives the separation between regime I and II. As discussed in detail in Section 4.1, this may mark the change from the aggregation of primary particles to the strengthening of the particle–particle bonds (see sketch). Fig. 1A corresponds to the last stage in the sketch. The sol state and the percolation process is not observable in this experiment.

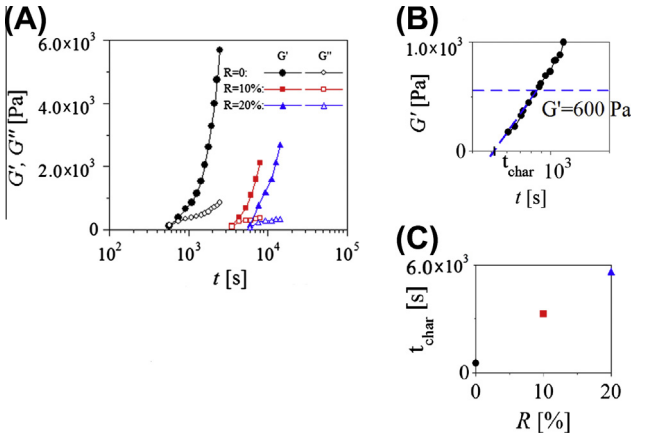

Fig. 3. (A): The evolution of the moduli with time for gels with increasing R, i.e., amount of additional water. The data was measured with time sweeps at $\gamma = 0.0005$, at $T = 23$ °C and $\omega = 10$ rad/s. (B): The characteristic time t_{char} was defined as the x-axis intercept of a logarithmic time dependence, which was fitted for the data $G' < 600$ Pa. (C) The characteristic time t_{char} increased with R.

Next, the time dependence of gel development was studied at temperatures $T = 23$, 30, 40, and 50 °C (Fig. 4). For temperatures up to 40 °C, the characteristic time increased with temperature. However at $T = 50$ °C the characteristic time decreased again to a value between that for 23 and 30 °C. The development of the gel at long times ($t > 3 \times 10^3$ s, as measured from the slope in the semi-log plots) continuously decreases with increasing temperature. At about $t = 5000$ s we observed a crossing of $G'(T = 50$ °C) with $G'(T = 30$ °C). This will be further discussed in Section 4.1.

3.2. Frequency dependence

The frequency sweeps revealed (Fig. 5A) that the storage modulus G' was constant at high frequencies (above about $\omega = 6$ rad/s), but frequency dependent at low frequencies. Typically the G' changed by about a factor of 2 between 0.1 and 6 rad/s. The increase of G' at low frequencies is at least 4.6 times larger than what would be expected from the pure aging of the gels (compare Fig. 2). Therefore, the frequency dependence of the sample can clearly be separated from its time dependence. Corresponding to this behavior we also observed a weak maximum in G'' for the gel with $R = 0$. The resolution limit of the rheometer leads to data scatter in G'' at frequencies beyond 30 rad/s. For this reason we limit the frequency range of the data shown here to the frequencies below 30 rad/s (see Fig. S1 for more details).

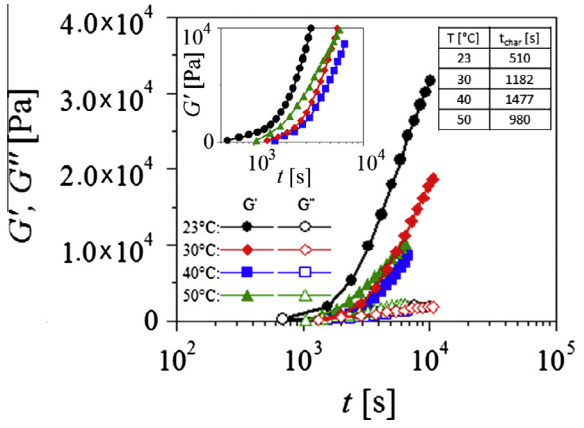

Fig. 4. The time dependence of moduli at different temperatures ($R = 0$, measured by time sweep, $\gamma = 0.0005$ and $\omega = 10$ rad/s). Inset: The data at low storage modulus range ($G' < 10^4$ Pa).

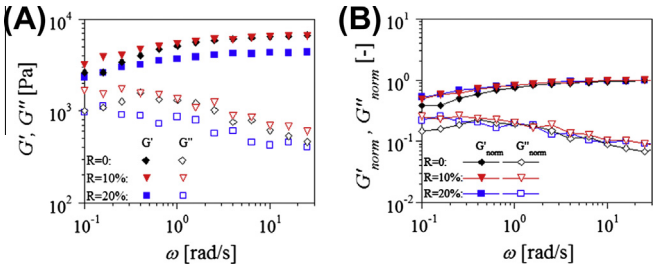

Fig. 5. (A): The frequency dependence of moduli of gels with various R. The data was measured with frequency sweeps, at $\gamma = 0.0005$, $T = 23$ °C, and $t = 4\ t_{char}$. (B): The same data normalized with $G'_{plateau} = G'(20$ rad/s), emphasizing the deviation from the plateau.

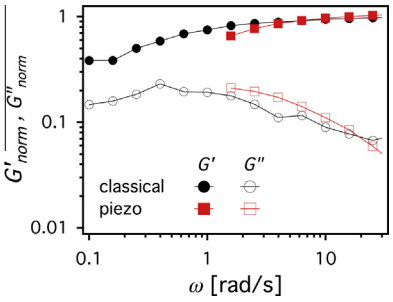

Fig. 6. Comparison of the frequency dependence of the normalized moduli measured with a classical and a piezo-rheometer.

This frequency dependence was present in all samples and also in samples from another batch of sodium silicate (data not shown). Details depended on composition, temperature and reaction time. To better visualize the deviation from the plateau value of G', we normalized the storage and loss moduli with the storage modulus plateau $G'_{plateau}$ at $\omega = 20$ rad/s. Since the storage modulus is 10 times larger than the loss modulus at high frequencies, the storage modulus is approximately equal to the absolute value of complex modulus, i.e., we normalized approximately with the absolute value of the complex modulus at high frequencies.

With this rescaling, the influence of water concentration on the frequency dependence became more easily visible (Fig. 5B). The deviation of the storage modulus at low frequencies from the plateau was more pronounced at lower water concentration. The corresponding normalized loss modulus G''_{norm} showed a maximum near $\omega = 0.4$ rad/s. Increasing R shifted the data curve of storage and loss moduli to lower frequency, see also Section 4.2. This frequency dependence of G' is more significant for higher temperatures and in younger gels (see Figs. S2 and S3 in supplementary data for details).

The frequency sweep measurement was repeated in the piezo-rheometer and the results from both rheometers agreed quite well (Fig. 6). The curves of normalized storage and loss moduli superimpose within our measurement accuracy. The slight deviation can be either due to minor differences in the composition of the sample or differences in the contact of the sample to the surfaces of the rheometers. Due to the similarities in the chemical structure, the silica gel adheres better to the glass substrate of the piezo-rheometer than to the metal cell of the Couette rheometer. The difference in adhesion was observed during the cleaning of both cells.

4. Discussion

4.1. Logarithmic time dependence of the storage modulus

Our time sweep data (Figs. 2–4) suggests that the structure of the precipitated silica gel develops in two phases. In each of them

storage modulus scaled with the logarithm of time. In agreement with previous studies [28], the slope of this logarithmic time dependence increased from the first to the second phase. Interestingly, such a behavior was known only for physical gels. Ronsin observed the 2-stage linear behavior with gelatin gel [18]. Also, Nijenhuis reported that the storage modulus of the physical gel of PVC plastisols follows logarithmic time dependence after some induction period [15]. In the rheo-optical study of physical gelation, a similar picture was presented [41]. Guo et al. attribute the two different slopes in the logarithmic time dependence to the increase of the number of cross-links at early times and internal reorganization at late times.

A similar gelation mechanism might explain the two-stage rheological behavior of the reactive silica gel. As shown in Fig. 2, before regime I the size of aggregates and their effect on rheology are not large enough to be detected by the rheological measurement, so there is no signal at the early time range. The growth of aggregates and formation of bonds between aggregates contribute essentially in regime I. At the intersection of the two trend lines with different slope (Fig. 2C), regime II begins, in which the strengthening of bonds and reorganization of the network dominates. However, to clarify this structural development, insight in the reaction equilibrium of the chemical reaction and the growth of the aggregates are needed and will be addressed in a further study.

Manley et al. [42] studied a gel of silica nano-particles that were destabilized by adding the divalent salt $MgCl_2$. A power law like growth of G' vs. time was observed. They explicitly noted the absence of structural changes in the gel and explained the time-dependent strength of colloidal gels with the coarsening process. The local elasticity increased because of bond formation between neighboring colloidal particles. The power law of G' vs. time is independent of the particle volume fraction. In contrast to the sample by Manley et al., our sample is a reactive system, in which the silica gel is in a reaction equilibrium between the formation and dissolution of chemical bonds. We attribute the different time dependence behavior of both silica gels to the difference in the properties of the particle–particle bonds.

The logarithmic time dependence of the modulus suggests that the system shares similarities with physical gels. As discussed in Section 1, a major difference between physical and chemical gel is that physical gelation is a (thermo-) reversible process, whereas traditional chemical gelation is not. In the case of reactive silica gel, although the silica bond is formed by a chemical reaction, the bond is reversible due to the finite solubility of silica at high pH. From pH value 9 to 12, the solubility increases dramatically from 0.015% to 0.5% [43]. In this sample with pH = 11.0, the dissolving of silica leads to bond breakage and thus relaxations in the system are possible. This process corresponds the aging of the gel, which is driven by the approach of the minimum of free energy, i.e., a more efficient distribution of bonds. Due to its physical-gel-like behavior, a structural relaxation in our reactive silica gel can be expected.

Quarch et al. reported a similar behavior for the temperature dependence of silica gel formation under alkaline conditions in a temperature range from 15 to 35 °C [21]. They explained the maximum in the characteristic (gelation) time with the finite solubility of silica at high pH (above 10.5). With increasing temperature, both the dissolution and formation kinetics accelerate. When the acceleration of formation dominates over that of the dissolution, a decrease in the characteristic time t_{char} is to be seen. In the inverse case one would expect an increase in t_{char}. The observed maximum in t_{char} may result from the compensation of both processes. Further, the frequency dependent signature of this accelerated reaction kinetics is seen in decreasing relaxations times with increasing temperature (Fig. 8, below).

In our study, we observe that the slope of the logarithmic time dependence at late times ($t > 3 \times 10^3$ s) depends monotonically on temperature (Fig. 4). The lower the temperature, the steeper the slope. This might be due to a temperature dependent shift of the reaction equilibrium. Further studies of the temperature dependent reaction kinetics in both directions, i.e., formation and dissociation of silica is needed to get a full understanding of this behavior.

4.2. Structure relaxation and fit of relaxation time

The experimental data clearly showed a frequency dependence of the storage modulus at low frequency (Section 3.2). Such a behavior has already been observed for dynamically arrested colloidal systems [44,45]. However this latter systems also showed a minimum of G'' at intermediate frequency that is not present in our reactive silica gel. This difference may be attributed to either the limited measurable frequency window or absence of polymer dynamics in our system. We attribute the frequency dependence to a structural relaxation inside the sample due to the reversibility of silica bonds at high pH (see above). In line with this interpretation, we found that the structural relaxation, as observed in the frequency dependence of the storage modulus, is more pronounced in the sample with lower water content, i.e., higher pH, at higher temperatures and in younger gels.

To get a more quantitative description of this relaxation process, we fitted this spectra with two different models, with which it was also checked whether the relaxation properties is dependent on the model. Like in dielectric spectroscopy, the Cole–Cole equation can be used to fit relaxation peaks. The modified Cole–Cole ansatz was adjusted for rheological application [46]. Additionally, we use the BSW function [47] to define the relaxation time spectrum in this sample. The logarithmic density function of the relaxation time spectrum $H(\tau)$, is defined by:

$$G(t) = \int_0^\infty \frac{H(\tau)}{\tau} e^{-\frac{t}{\tau}} d\tau \tag{3}$$

This describes the distribution and different weights of the relaxation times [46]. Both models describe well the linear viscoelastic behavior of polymer samples and their predictions are in good agreement with the experimental data from dynamical mechanical measurement [46–49]. In addition, both of them are consistent with the Kramers–Konig relation, the fundamental relation between the real and imaginary part of complex modulus. Both models allow for a simultaneous fit of G' and G''. Consequently, the fit is a consistency check for the measurement results.

However, the two models assume a different distribution of relaxation times in the sample. In the modified Cole–Cole function the distribution of relaxation times is centered around a characteristic relaxation time. Therefore it cannot directly be used to describe the terminal flow regime of polymer samples and modifications have to be applied [46]. In comparison, the BSW function is constructed such that it can be applied for describing the terminal behavior at low frequency. In the BSW model, the density of the relaxation mode drops to 0 when the time is longer than a certain value, above which the relaxation spectrum is cut. In this work, the terminal behavior of the system was not observable because it was outside the frequency range of the measurement. Therefore, the application limit of the modified Cole–Cole function does not influence the analysis in this study.

4.2.1. Relaxation time fitted by Cole–Cole function

The modified Cole–Cole equation [46,50] was applied to fit the data and to calculate the high frequency plateau of the storage modulus and the relaxation time.

$$G^* = \frac{G'_{plateau}(i\omega\tau_{CC})^{\alpha}}{1+(i\omega\tau_{CC})^{\alpha}} \qquad 0<\alpha\leqslant 1 \tag{4}$$

$$H(\tau) = \frac{G'_{plateau}}{\pi}\cdot\frac{(\frac{\tau}{\tau_{CC}})^{\alpha}\cdot\sin(\alpha\pi)}{1+2(\frac{\tau}{\tau_{CC}})^{\alpha}\cdot\cos(\alpha\pi)+(\frac{\tau}{\tau_{CC}})^{2\alpha}} \tag{5}$$

G^* is the complex modulus, which is measured directly with the rheometer. τ_{CC} is the characteristic relaxation time by modified Cole–Cole function. α describes the broadness of the corresponding distribution of relaxation times, the smaller α, the broader the distribution [46]. Using this equation, we implicitly assumed that the distribution of relaxation time is centered around τ_{CC}.

The fitting was performed using Origin 8.5 and is presented in an example of a gel with $R = 0$, measured at $T = 23$ °C and $t = 5\,t_{char}$ (Fig. 7). The fit line matches with the experimental data. The fitted storage modulus plateau $G'_{plateau}$ and characteristic relaxation time τ_{CC} are plotted as a function of water concentration R, temperature and aging time in Fig. 8.

With increasing R from 0% to 20%, the plateau value decreases and the relaxation time increases by more than a factor of two (Fig. 8A). Combined with the increase of characteristic time t_{char} with increasing R (Fig. 3C), we can conclude that the gel formation and structural relaxation both decelerated with increasing amount of water. The lower reactant concentration at higher R caused the decrease of storage modulus plateau and the slow-down of gel formation. Besides, the pH-value of the solution is slightly lower at higher R, corresponding lower solubility of silica could be a reason of the slower relaxation process.

For all investigated samples, the broadness parameter α of the Cole–Cole function was on the order of 0.5, indicating a broad distribution of relaxation times. The influence of water ratio on the broadness parameter α is insignificant and negligible in the range of standard deviation (Fig. 8B). The relaxation spectra $H(\tau)$ fitted with the modified Cole–Cole function and the BSW equation will be compared in Section 4.2.2.

The storage plateau value $G'_{plateau}$, characteristic relaxation time τ_{CC} and broadness parameter α decreased with increasing temperature (Fig. 8C and D). The decrease of the characteristic relaxation time implies a shorter bond life time. This might be correlated to a shift of the reaction equilibrium with temperature (Section 4.1). But complementary studies would be needed to understand the detailed correlation.

The plateau modulus $G'_{plateau}$ and the relaxation time τ_{CC} increase by more than a factor of 3 from $t/t_{char} = 5$ to 20 (Fig. 8E). Since the pH value of the sample stayed constant during the reaction (data not shown), the solubility of silica was also constant. Thus the dominating process can be assumed to be the strengthening of the network structure through reorganization of the network, leading to a better connectivity in the network and consequently slower relaxation.

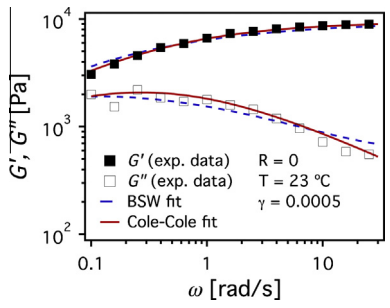

Fig. 7. The moduli of a gel example ($R = 0$ measured with $\gamma = 0.0005$, at $T = 23$ °C and $t = 5\,t_{char}$) are fitted with the modified Cole–Cole [46] (solid line, Section 4.2.1) and BSW function (dash line, Section 4.2.2).

4.2.2. Relaxation time calculated by BSW relaxation time spectrum

This model was used to describe the relaxation properties of mono-disperse linear polymers [47–49] and near-glass colloidal suspension [51,52]. In the equation, the relaxation process is expressed as the sum of β- and α-relaxation, which (for colloidal systems) originate from caging of the particle by the neighbors at short time and breakup of particle cages at long times in colloidal glass systems [51].

In our work, the fit of BSW equation was calculated by the IRIS graphics tool [40] with the following equation [51]:

$$H(\tau) = n_e G_N^0\left[\left(\frac{\tau}{\tau_{max}}\right)^{n_e}+\left(\frac{\tau}{\tau_0}\right)^{-n_g}\right] \qquad \tau\leqslant\tau_{max} \tag{6}$$

$$H(\tau) = 0 \qquad \tau>\tau_{max} \tag{7}$$

n_e: slope of the spectrum for the α-relaxation region
G_N^0: plateau modulus
τ_{max}: longest relaxation time
τ_0: time for β-relaxation state
n_g: slope of the spectrum for the β-relaxation region

Since the data at high frequency (over 30 rad/s) was not measured, we concentrated on the low frequency behavior. As the β relaxation part (i.e., the high-frequency term $(\tau/\tau_0)^{-n_g}$) could be ignored, we use a simplified version of Eq. (6) in the fitting procedure. The decreased number of parameters (three instead of six) also reduced the uncertainties in the fits.

$$H(\tau) = n_e G_N^0\left(\frac{\tau}{\tau_{max}}\right)^{n_e} \qquad \tau\leqslant\tau_{max} \tag{8}$$

$$H(\tau) = 0 \qquad \tau>\tau_{max} \tag{9}$$

The comparison between the fit curves with modified Cole–Cole and BSW is displayed in Fig. 9. The characteristic relaxation time τ_{CC} from Cole–Cole fit and the maximum relaxation time τ_{max} from BSW fit are compared for various temperatures (Fig. 9A) and reaction times (Fig. 9C).

Despite differences in the absolute numbers, the general tendency is the same by the results from both models. A possible origin of these differences is the different distribution of relaxation times. However, it was observed (e.g., Fig. 9D) that a broader distribution of relaxation time for Cole–Cole corresponds to a smaller slope of distribution modulus $H(\tau)$ in the BSW fit. Thus the conclusions are independent of the actual model that was used for the analysis.

In the BSW fit data, there was a clear tendency for the relaxation modulus $H(\tau)$ to increase with relaxation time τ. In contrast, for a chemical (polymer) gel, $H(\tau)$ is expected to decrease with time [53]. However, the relaxation properties of the reactive silica gel are similar to weak colloidal gels at low frequency [44,45]. For colloidal gels, the structural reorganization occurs on the large scale, which corresponds to the relaxation process at long time, i.e., low frequency. Similarly, the dissolution and formation of the silica bonding allows the rearrangement of the reactive silica gel on the large scale. Such processes contribute to the relaxation process at long relaxation times.

5. Conclusions

In this contribution we investigated the rheological behavior of aggregated colloidal silica nano-particles at high pH. The

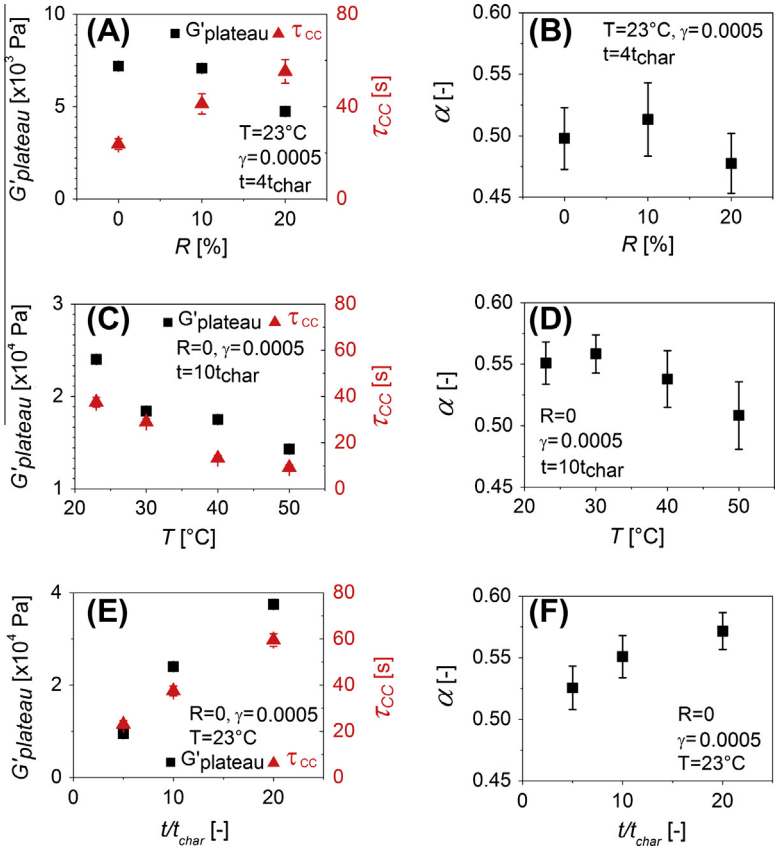

Fig. 8. The results from fits with the modified Cole–Cole function. The dependence of the fitted storage modulus plateau $G'_{plateau}$ and characteristic relaxation time τ_{CC} on water concentration R (A), temperature T (C), and time t/t_{char} (E). The broadness parameter α is plotted as function same parameters (B), (D) and (F).

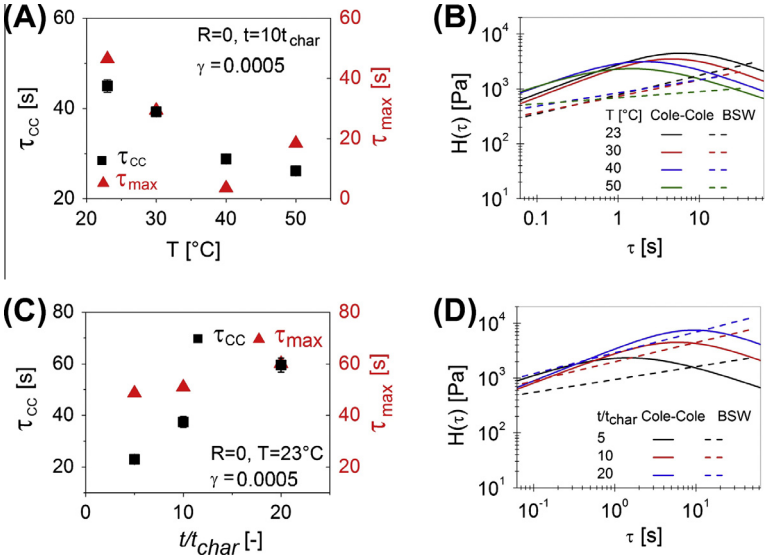

Fig. 9. Comparison of the two models used: The dependence of relaxation time τ_{CC} from the fit to the modified Cole–Cole function and maximum relaxation time τ_{max} as calculated from the BSW function on the temperature (A) and time t/t_{char} (C). The relaxation modulus $H(\tau)$ is plotted against relaxation time τ for the corresponding temperatures (B) and times t/t_{char} (D).

nano-particles were formed through the precipitation of silica from sodium silicate by mixing with diluted sulfuric acid. A particularity of this material is the high pH value that allowed for a finite solubility of silica in the reaction mixture [28]. Consequently, a reaction equilibrium between the bond dissolution and formation was expected. This reactive silica gel exhibited behavior known from physical and colloidal gels: a logarithmic time dependence of the storage modulus [15,18] and a low frequency structural relaxation [44]. Two stages with different regimes were observed in the temporal evolution of the storage modulus of the gel. We attribute these two regimes to (I) the formation of aggregates from primary particles and bonding at short

times and (II) further growth of the bonds and restructuring at long times.

A structural relaxation was evident from the frequency dependent measurements. The storage modulus G' exhibited frequency dependence below 6 rad/s. A similar behavior was observed for colloidal gels [44]. The microscopic origin of the structural relaxation is assumed to be the finite solubility of silica at high pH. Effectively this finite solubility leads to a finite bond life time and opens the way for a restructuring of this gel on the micro-scale, i.e., for a structural relaxation. Due to assumed the molecular scale of this relaxation, a detailed study of this mechanism is beyond the scope of the present study. A systematic analysis showed that the structural relaxation mode is more pronounced in concentrated samples, at higher temperatures and in younger gels.

The experimental data of the frequency dependent mechanical moduli could be fitted with models that allow for a calculation of relaxation times and modulus. A modified Cole–Cole equation [46] and the BSW [47] function were used for this purpose with comparable results. Both models agree on how the properties of the low frequency relaxation depend on the experimental parameters. The extracted relaxation time is longer for higher water concentrations, lower temperatures, and older gels. The distribution of relaxation times turned out to be broader for higher temperatures and younger gels but independent of the concentration.

The structural relaxation due to the reaction equilibrium described in this work illustrates the flexibility of this material, although it is made out of a rigid material like silica. This flexibility can interfere with applied external fields, e.g., mechanical stresses, and open the way to generate a material whose mechanical properties can be tuned through the applied stress on the material during the production process. To follow this further is, however, beyond the scope of the present manuscript and will be dealt with in a future work.

Acknowledgments

We are grateful to Marcel Roth, Doris Vollmer, and Matthias Kind for the inspiring discussions. M.W. also thanks the Deutsche Forschungsgemeinschaft (SPP 1273, "Kolloidverfahrenstechnik") and the international Max-Planck Research School (IMPRS) for financial support.

Appendix A. Supplementary material

Supplementary data associated with this article can be found, in the online version, at http://dx.doi.org/10.1016/j.jcis.2013.09.035.

References

[1] E. Zaccarelli, J. Phys.: Condens. Matter 19 (32) (2007) 323101.
[2] K.A. Dawson, Curr. Opin. Colloid Interface Sci. 7 (3–4) (2002) 218–227.
[3] F. Sciortino, P. Tartaglia, Adv. Phys. 54 (6–7) (2005) 471–524.
[4] P.A. Smith, G. Petekidis, S.U. Egelhaaf, W.C.K. Poon, Phys. Rev. E 76 (4) (2007) 041402.
[5] S.B. Lindstrom, T.E. Kodger, J. Sprakel, D.A. Weitz, Soft Matter 8 (13) (2012) 3657–3664.
[6] J.E. Martin, D. Adolf, Annu. Rev. Phys. Chem. 42 (1991) 311–339.
[7] P.J. Flory, Principles of Polymer Chemistry, Cornell University Press, 1953.
[8] P.-G. d. Gennes, Scaling Concepts in Polymer Physics, Cornell University Press, 1979.
[9] P.N. Segr, V. Prasad, A.B. Schofield, D.A. Weitz, Phys. Rev. Lett. 86 (26) (2001) 6042–6045.
[10] C.J. Rueb, C.F. Zukoski, J. Rheol. 41 (2) (1997) 197–218.
[11] M.J. Solomon, P. Varadan, Phys. Rev. E 63 (5) (2001) 051402.
[12] F. Chambon, H.H. Winter, J. Rheol. 31 (8) (1987) 683–697.
[13] P. Matricardi, M. Dentini, V. Crescenzi, S.B. Ross-Murphy, Carbohydr. Polym. 27 (3) (1995) 215–220.
[14] D.F. Hodgson, E.J. Amis, J. Non-Cryst. Solids 131 (1991) 913–920.
[15] K.T. Nijenhuis, H.H. Winter, Macromolecules 22 (1) (1989) 411–414.
[16] H. Tanaka, S. Jabbari-Farouji, J. Meunier, D. Bonn, Phys. Rev. E 71 (2) (2005) 021402.
[17] A. Parker, V. Normand, Soft Matter 6 (19) (2010) 4916–4919.
[18] O. Ronsin, C. Caroli, T. Baumberger, Phys. Rev. Lett. 103 (13) (2009) 138302.
[19] S.Z. Ren, C.M. Sorensen, Phys. Rev. Lett. 70 (11) (1993) 1727–1730.
[20] R.K. Iler, The Chemistry of Silica, John Wiley & Sons, Inc., 1979.
[21] K. Quarch, M. Kind, Chem. Eng. Technol. 33 (6) (2010) 1034–1039.
[22] O. Ruff, P. Mautner, Angew. Chem. 40 (15) (1927) 428–434.
[23] C.B. Hurd, C.L. Raymond, P.S. Miller, J. Phys. Chem. 38 (5) (1934) 663–674.
[24] C.B. Hurd, A.J. Marotta, J. Am. Chem. Soc. 62 (1940) 2767–2770.
[25] C.B. Hurd, R.C. Pomatti, J.H. Spittle, F.J. Alois, J. Am. Chem. Soc. 66 (1944) 388–390.
[26] C.J. Brinker, G.W. Scherer, Sol–Gel Science, Elsevier Science, 1989.
[27] P.C. Carman, Trans. Faraday Soc. 36 (1940) 0964–0972.
[28] M. Prasad, S.M. Mehta, J.B. Desai, J. Phys. Chem. 36 (5) (1932) 1384–1390.
[29] G.W. Scherer, J. Sol–Gel Sci. Technol. 1 (2) (1994) 169–175.
[30] G.W. Scherer, J. Sol–Gel Sci. Technol. 2 (1) (1994) 199–204.
[31] G.W. Scherer, Langmuir 12 (5) (1996) 1109–1116.
[32] G.W. Scherer, J. Non-Cryst. Solids 142 (0) (1992) 18–35.
[33] S. Corezzi, D. Fioretto, D. Puglia, J.M. Kenny, Macromolecules 36 (14) (2003) 5271–5278.
[34] P.D. Patel, W.B. Russel, J. Colloid Interface Sci. 131 (1) (1989) 201–210.
[35] S.R. Kamath, A. Proctor, Cereal Chem. 75 (4) (1998) 484–487.
[36] R. Bartolino, G. Durand, Phys. Rev. Lett. 39 (21) (1977) 1346–1349.
[37] K. Okano, J. Yamamoto, Jpn. J. Appl. Phys., Part 1 29 (6) (1990) 1149–1150.
[38] P. Martinoty, J.L. Gallani, D. Collin, Phys. Rev. Lett. 81 (1) (1998) 144–147.
[39] M. Roth, M. D'Acunzi, D. Vollmer, G.K. Auernhammer, J. Chem. Phys. 132 (2010) 124702.
[40] M. Mours, H.H. Winter, Rheol. Acta 33 (5) (1994) 385–397.
[41] L. Guo, R.H. Colby, C.P. Lusignan, A.M. Howe, Macromolecules 36 (26) (2003) 10009–10020.
[42] S. Manley, B. Davidovitch, N.R. Davies, L. Cipelletti, A.E. Bailey, R.J. Christianson, U. Gasser, V. Prasad, P.N. Segre, M.P. Doherty, S. Sankaran, A.L. Jankovsky, B. Shiley, J. Bowen, J. Eggers, C. Kurta, T. Lorik, D.A. Weitz, Phys. Rev. Lett. 95 (4) (2005) 048302.
[43] G.B. Alexander, W.M. Heston, R.K. Iler, J. Phys. Chem. 58 (6) (1954) 453–455.
[44] M. Laurati, G. Petekidis, N. Koumakis, F. Cardinaux, A.B. Schofield, J.M. Brader, M. Fuchs, S.U. Egelhaaf, J. Chem. Phys. 130 (13) (2009) 134907.
[45] K.N. Pham, G. Petekidis, D. Vlassopoulos, S.U. Egelhaaf, W.C.K. Poon, P.N. Pusey, J. Rheol. 52 (2) (2008) 649–676.
[46] C. Friedrich, H. Braun, Rheol. Acta 31 (4) (1992) 309–322.
[47] M. Baumgaertel, A. Schausberger, H.H. Winter, Rheol. Acta 29 (5) (1990) 400–408.
[48] G.A. Carri, H.H. Winter, Rheol. Acta 36 (3) (1997) 330–344.
[49] C. Friedrich, W. Waizenegger, H.H. Winter, Rheol. Acta 47 (8) (2008) 909–916.
[50] N.W. Tschoegl, The Phenomenological Theory of Linear Viscoelastic Behavior: An Introduction, Springer-Verlag, 1989.
[51] H.H. Winter, M. Siebenbuerger, D. Hajnal, O. Henrich, M. Fuchs, M. Ballauff, Rheol. Acta 48 (7) (2009) 747–753.
[52] H.H. Winter, Macromolecules 46 (6) (2013) 2425–2432.
[53] H. Winter, M. Mours, Rheology of Polymers Near Liquid–Solid Transitions Neutron Spin Echo Spectroscopy Viscoelasticity Rheology, Advances in Polymer Science, vol. 134, Springer, Berlin/Heidelberg, 1997.